FRONTIERS OF PHYSICS

TOPICAL REVIEW
Volume 18 / Issue 6 / 64602 / 2023

The factorization-assisted topological-amplitude approach and its applications

Qin Qin[1,†], Chao Wang[2,‡], Di Wang[3,§], Si-Hong Zhou[4,#]

1 School of Physics, Huazhong University of Science and Technology, Wuhan 430074, China
2 Faculty of Mathematics and Physics, Huaiyin Institute of Technology, Huaian 223001, China
3 Department of Physics, Hunan Normal University, Changsha 410081, China
4 School of Physical Science and Technology, Inner Mongolia University, Hohhot 010021, China
E-mail: †qqin@hust.edu.cn, ‡chaowang@nankai.edu.cn, §wangdi@hunnu.edu.cn, #shzhou@imu.edu.cn
Received February 23, 2023; accepted June 12, 2023

ABSTRACT

Heavy meson decays provide an important platform for studies of both QCD and electroweak dynamics, which may contain some portals to understanding of nonperturbative QCD and physics beyond the Standard Model. The factorization-assisted topological-amplitude approach was proposed to study two-body non-leptonic D meson decays, where a promising QCD inspired approach from first principles is still missing. It was also applied to B meson decays whose subleading power contributions are difficult to calculate. By factorizing topological amplitudes into short distance Wilson coefficients and long distance hadronic matrix elements either to be calculated or to be parameterized, it provides an effective framework to extract information of nonperturbative dynamics involved. With important flavor $SU(3)$ breaking effects taken into account, the data of the decay branching ratios (and also CP asymmetries in B decays) can be fitted well. The extracted amplitudes were further applied to make predictions for other observables, such as CP asymmetries in D decays, mixing parameters in the D^0–$\bar{D}^0$ system. By this review, we will describe the formulation of the factorization-assisted topological-amplitude approach and summarize its applications in D and B meson decays and highlight some of its achievements.

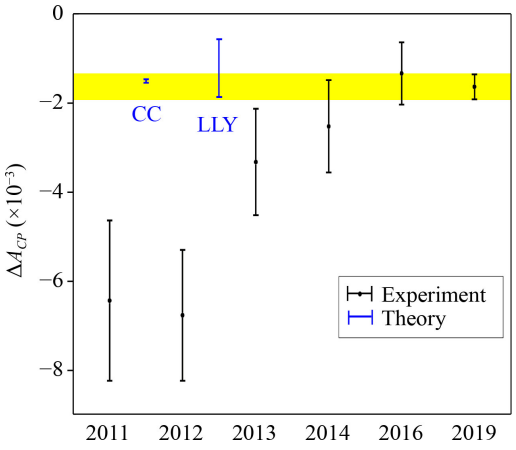

Keywords heavy meson decay, factorization-assisted topological-amplitude approach, $SU(3)$ breaking

Contents

1 Introduction

Non-leptonic heavy meson decay provides an ideal platform

Higher Education Press

arXiv: 2111.14472
https://doi.org/10.1007/s11467-023-1321-3

to test the Standard Model (SM) and search for new physics. Abundant data of the B and D meson decays have been collected by BaBar, Belle (II), BESIII and LHCb experiments in the last couple of decades [1]. Just recently, the LHCb Collaboration observed the CP violation in the charm sector with 5.3σ in 2019 [2], which is a event in the heavy quark physics. In theory, QCD inspired approaches based on heavy quark expansion have been developed to calculate the non-leptonic B meson decays, such as QCD factorization (QCDF) [3–5], perturbative QCD approach (PQCD) [6–9], and soft-collinear effective theory (SCET) [10–12]. Although significant progresses have been made within these approaches, systematic calculation of $(\Lambda_{\rm QCD}/m_b)^n$ power corrections is still challenging for all of them. For D meson decays, the situation is even worse because of the poor convergence with the large expansion parameters $\alpha_s(m_c)$ and $\Lambda_{\rm QCD}/m_c$. As a result, it is difficult to calculate the D decay amplitudes from first principles of QCD.

One idea is to extract the dynamics of D meson decays from data based on some model assumptions. One of the popular methods is the topological diagram approach [13–21]. In this approach, the topological diagrams are classified according to the topologies in the flavor flow of weak decay diagrams and all strong interaction effects induced implicitly. It provides a framework to analyze nonperturbative effects by data fitting. However, the usual global fitting is based on the flavor symmetric topological diagrams, with the flavor $SU(3)$ breaking effects not included. The $SU(3)$ breaking effects should be around 20% and turn out to be nonnegligible even in B meson decays [22]. It leads to the inability of interpreting the branching fractions, especially in the singly Cabibbo-suppressed D decays. The topological diagram approach can include the flavor symmetry breaking effects by considering a linear $SU(3)$ breaking [23], but it will induce too many parameters to fit limited data which causes very large uncertainties.

The factorization-assisted topological-amplitude approach (FAT) was proposed in Refs. [24–27] parameterizing the nonperturbative contributions in the two-body non-leptonic D/B decays, trying to decode the involved $SU(3)$ breaking effects. In this framework, the factorization hypothesis is used to calculate topological amplitudes that are factorized into two parts: the short-distance Wilson coefficients and the long-distance hadronic matrix elements. The nonfactorizable contributions are determined by the experimental data. It is expected that the dominant $SU(3)$ breaking effects are effectively summarized by several parameters. It turns out that the FAT can fit the data very well, including those of the D/B decays into two pseudoscalar mesons (PP), one pseudoscalar meson and one vector meson (PV), and two vector mesons (VV). Furthermore, the extracted amplitudes information can be used to calculate other observables. For example, the FAT prediction on the CP asymmetry difference $\Delta A_{CP} \equiv A_{CP}(D^0 \to K^+K^-) - A_{CP}(D^0 \to \pi^+\pi^-)$ was given in 2012 [24], which was recently confirmed by the LHCb measurement [2]. Besides, the FAT approach can also be applied to study other topics such as neutral D mixing and K^0_S–K^0_L asymmetry. In this review, we will briefly introduce the basic ideas of FAT approach and highlight the achievements it has achieved.

The rest of this paper is organized as follows. In Section 2, we review the basic ideas and the results of the FAT approach in the branching fractions of D meson decays. In Section 3, we discuss the CP violation and related topics in the charm sector. In Section 4, the application of FAT approach in the B meson decays is reviewed. Section 5 contains a summary and outlook.

2 Branching fractions of charm decays

According to the quark transition of the weak operators, there are four types of amplitudes contributing to the two-body D decays — the color-favored tree amplitude T, the color-suppressed amplitude C, the W-exchange amplitude E and the W-annihilation amplitude A, as displayed as the corresponding four topological diagrams in Fig. 1. In the FAT approach, the two-body non-leptonic D meson decays are formulated in a way that the short- and long-distance dynamics are separated with the former calculable and the latter parameterized to be determined by data. The effective Hamiltonian of charm decay in the SM can be written as

$$\begin{aligned}\mathcal{H}_{eff} =& \frac{G_{\rm F}}{\sqrt{2}} V_{\rm CKM}\left[C_1(\mu)Q_1(\mu) + C_2(\mu)Q_2(\mu)\right] + \text{H.c.},\\ Q_1 =& \bar{u}_\alpha \gamma_\mu(1-\gamma_5) q_{2\beta} \bar{q}_{1\beta}\gamma^\mu(1-\gamma_5)c_\alpha,\\ Q_2 =& \bar{u}_\alpha \gamma_\mu(1-\gamma_5) q_{2\alpha} \bar{q}_{1\beta}\gamma^\mu(1-\gamma_5)c_\beta,\end{aligned} \tag{1}$$

where $G_{\rm F}$ denotes the Fermi coupling constant, $V_{\rm CKM}$ is the products of the Cabibbo–Kobayashi–Maskawa (CKM) matrix elements, $C_{1,2}$ are the Wilson coefficients, α, β are the color indices. The physics above the scale $\mu \sim m_c$ is handled by the Wilson coefficients $C_{1,2}(\mu)$, and the physics below μ is handled by the hadronic matrix elements of the current–current operators $\langle M_1 M_2|O_{1,2}|D\rangle$. In the FAT approach, the factorizable parts of the four amplitudes are either calculated by the naive factorization as the products of the corresponding decay constants and form factors, or neglected owing to the color suppression or the helicity suppression. The non-factorizable parts are parameterized with non-perturbative parameters and extracted by fitting.

The topological amplitudes of the $D \to PP$ decay in the FAT are [24]

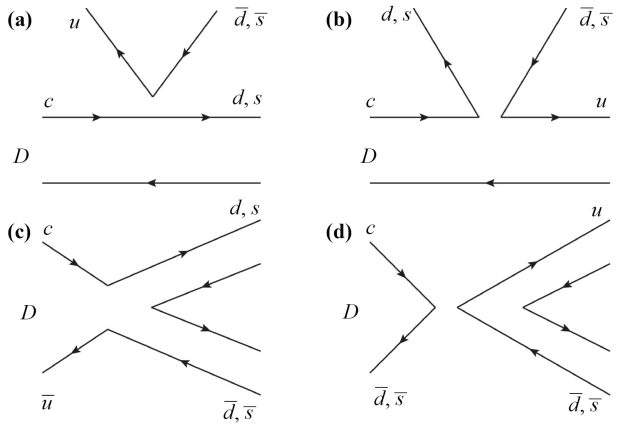

Fig. 1 Topological tree diagrams contributing to the two-body non-leptonic D decays with **(a)** the color-favored penguin amplitude T, **(b)** the color-suppressed penguin amplitude C, **(c)** the gluon-exchange penguin amplitude E, and **(d)** the gluon-annihilation penguin amplitude A. The diagrams are reproduced from Ref. [24].

$$T=\frac{G_{\rm F}}{\sqrt{2}}V_{\rm CKM}a_1(\mu)f_{P_2}(m_D^2-m_{P_1}^2)F_0^{D\to P_1}(m_{P_2}^2), \quad (2)$$

$$C=\frac{G_{\rm F}}{\sqrt{2}}V_{\rm CKM}a_2(\mu)f_{P_2}(m_D^2-m_{P_1}^2)F_0^{D\to P_1}(m_{P_2}^2), \quad (3)$$

$$E=\frac{G_{\rm F}}{\sqrt{2}}V_{\rm CKM}C_2(\mu)\chi_{q,s}^E e^{i\phi_{q,s}^E}f_D m_D^2\Big(\frac{f_{P_1}f_{P_2}}{f_\pi^2}\Big), \quad (4)$$

$$A=\frac{G_{\rm F}}{\sqrt{2}}V_{\rm CKM}C_1(\mu)\chi_{q,s}^A e^{i\phi_{q,s}^A}f_D m_D^2\Big(\frac{f_{P_1}f_{P_2}}{f_\pi^2}\Big), \quad (5)$$

with

$$\begin{aligned}a_1(\mu)=&C_2(\mu)+\frac{C_1(\mu)}{N_c},\\ a_2(\mu)=&C_1(\mu)+C_2(\mu)[\frac{1}{N_c}+\chi^C e^{i\phi^C}].\end{aligned} \quad (6)$$

$C_{1,2}(\mu)$ are the Wilson coefficients at the scale of $\mu=\sqrt{\Lambda m_D(1-r_2^2)}$ for T and C diagrams, and $\mu=\sqrt{\Lambda m_D(1-r_1^2)(1-r_2^2)}$ for E and A diagrams, with $r_i=m_{P_i}/m_D$. In T and C diagrams, P_1 is the pseudoscalar meson transited from the D decay and P_2 is the emitted meson. T diagram is calculated in the factorization hypothesis, f_i and F_0 are the decay constants and transition form factors, respectively. The nonfactorizable contributions in the C diagram, resulting from the final-state interactions, are parametrized as magnitude and strong phase as $\chi^C e^{i\phi^C}$. E and A diagrams are dominated by the nonfactorizable contributions, parametrized as $\chi_{q,s}^{E,A}e^{i\phi_{q,s}^{E,A}}$. The subscripts q and s stand for the quark pairs produced from the vacuum as the u, d quarks or the s quark. Because of the fact that the pion boson is a Nambu–Goldstone boson and quark–antiquark bound state simultaneously, a Glauber phase factor [28, 29], e^{iS_π}, is introduced for each pion involved in the non-factorizable contributions of E and A amplitudes. The topological amplitudes of the $D\to PV$ mode are [25]

$$\begin{aligned}T_P[C_P]=&\frac{G_{\rm F}}{\sqrt{2}}V_{\rm CKM}a_1^P(\mu)[a_2^P(\mu)]f_V m_V F_1^{D\to P}(m_V^2)\\ &\times 2(\varepsilon_V\cdot p_D),\end{aligned} \quad (7)$$

$$\begin{aligned}T_V[C_V]=&\frac{G_{\rm F}}{\sqrt{2}}V_{\rm CKM}a_1^V(\mu)[a_2^V(\mu)]f_P m_V A_0^{D\to V}(m_P^2)\\ &\times 2(\varepsilon_V\cdot p_D),\end{aligned} \quad (8)$$

$$E_{P,V}=\frac{G_{\rm F}}{\sqrt{2}}V_{\rm CKM}C_2(\mu)\chi_{q,s}^E e^{i\phi_{q,s}^E}f_D m_D\frac{f_P f_V}{f_\pi f_\rho}(\varepsilon_V\cdot p_D), \quad (9)$$

$$A_{P,V}=\frac{G_{\rm F}}{\sqrt{2}}V_{\rm CKM}C_1(\mu)\chi_{q,s}^A e^{i\phi_{q,s}^A}f_D m_D\frac{f_P f_V}{f_\pi f_\rho}(\varepsilon_V\cdot p_D), \quad (10)$$

where the subscript P in T_P and C_P represents the topologies with a transited pseudoscalar meson and an emitted vector boson, while the subscript V in T_V and C_V stands for the transited vector meson and emitted pseudoscalar meson diagrams. For the annihilation-type diagrams, the subscripts of $E_{P,V}$ and $A_{P,V}$ stand for the anti-quark from charm decay entering in the pseudoscalar meson or the vector meson. One can refer to Refs. [24, 25] for more details.

The FAT formulation covers the flavor $SU(3)$ breaking effects in several aspects. Firstly, the decay constants and transition form factors include the $SU(3)$ breaking effects. Secondly, the energy scale μ is set to depend on final states to describe the different energy release. Thirdly, two nonperturbative parameters are introduced for the case of quark pair producing from vacuum as u, d quarks or s quark in topologies E and A. Fourthly, the Glauber gluon effects are considered in the pion involved channels. Finally, the phase spaces are different for different decay channels. Compared to the $SU(3)$ symmetric topological diagram scheme in which only the $SU(3)$ breaking due to phase space is considered, the FAT parameterization include abundant sources of the $SU(3)$ breaking.

The fits to the data of branching ratios for the PP and PV channels are performed in Refs. [24] and [25], respectively. An update was made by [33] for the neutral D^0 meson decays. In order to show the relative weights of different topologies, the best-fit values of nonperturbative parameters taken from Refs. [24, 25] are as follows:

Table 1 Comparison for FAT predictions and experimental data of branching ratios of the $D \to PP$ decays in units of permill. The data without quote are taken from PDG [1] and only the experimental results updated after the theoretical predictions are listed.

Channel	FAT	Data	Channel	FAT	Data
$D^0 \to K^0_S K^0_S$	0.15 ± 0.04 [33]	0.141 ± 0.005	$D^0 \to \pi^0\eta$	0.74 ± 0.03 [33]	0.63 ± 0.06
$D^0 \to \pi^0\eta'$	1.08 ± 0.05 [33]	0.92 ± 0.10	$D^0 \to \eta\eta$	1.86 ± 0.06 [33]	2.11 ± 0.19
$D^0 \to \eta\eta'$	1.05 ± 0.08 [33]	1.01 ± 0.19	$D^0 \to \pi^+\pi^-$	1.44 ± 0.02 [33]	1.454 ± 0.024
$D^0 \to K^+K^-$	4.05 ± 0.07 [33]	4.08 ± 0.06	$D^0 \to K^-\pi^+$	39.3 ± 0.4 [33]	39.47 ± 0.30
$D^0 \to K^0_S\pi^0$	12.1 ± 0.4 [33]	12.40 ± 0.22	$D^0 \to K^0_S\eta$	4.8 ± 0.3 [33]	5.13 ± 0.14 [34]
$D^0 \to K^0_S\eta'$	9.8 ± 0.5 [33]	9.49 ± 0.41 [34]	$D^+ \to \pi^+\pi^0$	0.89 [24]	1.247 ± 0.033
$D^+ \to K^+\pi^0$	0.197 [24]	0.208 ± 0.021	$D^+ \to \pi^+\eta$	3.39 [24]	3.77 ± 0.09
$D^+ \to K^+\eta$	0.066 [24]	0.125 ± 0.016	$D^+ \to \pi^+\eta'$	4.58 [24]	4.97 ± 0.19
$D^+ \to K^+\eta'$	0.114 [24]	0.185 ± 0.020	$D^+ \to \pi^+K^0_S$	16.2 [24]	15.62 ± 0.31
$D^+ \to K^+K^0_S$	2.98 [24]	3.04 ± 0.09	$D^+_s \to \pi^+\pi^0$	0 [24]	0.037 ± 0.059 [35]
$D^+_s \to \pi^0K^+$	0.67 [24]	0.74 ± 0.05	$D^+_s \to \pi^+K^0_S$	1.105 [24]	1.10 ± 0.05
$D^+_s \to K^+K^0_S$	15.03 [24]	14.53 ± 0.35	$D^+_s \to \pi^+\eta$	16.5 [24]	16.8 ± 0.9
$D^+_s \to K^+\eta$	1.0 [24]	1.73 ± 0.08	$D^+_s \to \pi^+\eta'$	34.4 [24]	39.4 ± 2.5
$D^+_s \to K^+\eta'$	1.92 [24]	2.64 ± 0.24			

$D \to PP$ mode,

$$\begin{aligned}&\Lambda = 0.56\,\text{GeV},\ \ \chi_{nf} = -0.59,\ \ \chi^E_q = 0.11,\ \ \chi^E_s = 0.18,\\ &\chi^A_q = 0.12,\ \ \chi^A_s = 0.17,\ \ S_\pi = -0.50,\ \ \phi = -0.62,\\ &\phi^E_q = 4.80,\ \ \phi^E_s = 4.23,\ \ \phi^A_q = 4.06,\ \ \phi^A_s = 3.48;\end{aligned} \tag{11}$$

$D \to PV$ mode,

$$\begin{aligned}&\Lambda = 0.44\,\text{GeV},\ \ \chi^C_P = -0.40,\ \ \phi^C_V = -0.25,\ \ \chi^E_q = 0.25,\\ &\chi^E_s = 0.29,\ \ \chi^A_q = 0.11,\ \ \chi^A_s = 0.10,\ \ S_\pi = -0.96,\\ &\phi^C_P = -0.53,\ \ \chi^C_V = -0.53,\ \ \phi^E_q = 1.73,\ \ \phi^A_q = -0.35,\\ &\phi^E_s = 3.11,\ \ \phi^A_s = 1.60.\end{aligned} \tag{12}$$

The fitted values support the relation $T \geq C \geq E \geq A$ in both $D \to PP$ and $D \to PV$ modes. The consistency between the fitted results and the experimental data indicates that both the perturbative and non-perturbative dynamics of the two-body non-leptonic D meson decays, especially the flavor $SU(3)$ breaking effects, are well handled by the FAT approach. The non-factorizable magnitude parameters, which should be power suppressed in the heavy quark expansion, turn out to be not so small compared to the factorizable ones. This confirms our expectation that the heavy quark expansion does not work well for D meson decays, which is one of the main motivations of the FAT approach.

One important achievement of the FAT approach is that it provided a solution to the long-standing $\pi\pi$–KK puzzle — the measured $D^0 \to K^+K^-$ branching ratio is about three times the $D^0 \to \pi^+\pi^-$ branching ratio, while the previous theoretical calculations predicted a smaller branching ratio for $D^0 \to K^+K^-$. As pointed out in Ref. [15], the W-exchange amplitudes in the two channels must have not only different magnitudes but also different strong phases to give the correct branching ratios. In the FAT approach, different decay constants and form factors can account for different magnitudes. More importantly, the Glauber gluon effects involved in the $\pi^+\pi^-$ channel appropriately rotate the phase angle in the E amplitude to give a correct prediction for the $\pi^+\pi^-$ branching ratio and the correct relation between the $\pi\pi$–KK channels. This is another evidence that the $SU(3)$ breaking effects are well under control in the FAT approach, which is crucial to the study of the D^0–$\bar{D}^0$ mixing, which will be discussed in the next section.

In the global fit of the PV channels [25], there was one channel $D^+_s \to \rho^+\omega$ whose FAT fit result was never consistent with the PDG value $\mathcal{B}(D^+_s \to \rho^+\omega) = (11.7 \pm 1.8)\%$ at that time [30]. The FAT prediction 1.6%–1.7% is more consistent with a new measurement by the CLEO-c, $(5.6 \pm 1.1)\%$ [31], which was later confirmed by a BESIII measurement $(5.8 \pm 1.4 \pm 0.4)\%$ [32].

After the publications of [24, 25, 33], the branching ratios of many observed D meson decay channels have been remeasured with higher precisions and also many new D meson decay channels have been discovered by experiments. We list their results in Tables 1 and 2 for the PP and PV channels, respectively, compared to the FAT predictions. They are basically in consistence with each other.

3 *CP* violation and related topics in charm

Except for predictions of the branching fractions, the FAT approach also provides a prescription that the penguin amplitudes can be related to the tree amplitudes

Table 2 Comparison for FAT predictions and experimental data of branching ratios of the $D \to PV$ decays in units of permill. The data without quote are taken from PDG [1] and only the experimental results updated after the theoretical predictions are listed.

Channel	FAT	Data	Channel	FAT	Data
$D^0 \to \eta\omega$	2.1 ± 0.1 [33]	1.98 ± 0.18	$D^0 \to \eta\overline{K}^{*0}$	6.1 ± 1.0 [33]	$13.4^{+1.2}_{-0.9}$
$D^0 \to \pi^0\phi$	1.4 ± 0.1 [33]	1.34 ± 0.12	$D^0 \to \eta\phi$	0.18 ± 0.04 [33]	0.184 ± 0.012
$D^+ \to \pi^+\phi$	5.65(5.65) [25]	5.70 ± 0.14	$D^+ \to K^+\phi$	0.001(0.002) [25]	< 0.021
$D^+ \to K^+\omega$	0.09(0.07) [25]	$0.057^{+0.025}_{-0.021}$	$D^+ \to K^0_S K^{*+}$	5.5(5.5) [25]	2.89 ± 0.30
$D_s^+ \to \eta'\rho^+$	17(16) [25]	58 ± 15	$D_s^+ \to \pi^+\omega$	3.0(2.6) [25]	1.92 ± 0.30
$D_s^+ \to K^+\omega$	0.6(0.07) [25]	0.87 ± 0.25			

and then the CP asymmetries in the D meson decays are predicted. Four topological penguin diagrams contributing to the two-body non-leptonic D decays are shown in Fig. 2[1]. In the FAT approach, penguin amplitudes P and P_C as well as the nonfactorizable contributions to P_E and P_A are estimated by replacement of the Wilson coefficients of the corresponding tree amplitudes in which the nonperturbative parameters have been determined by fitting branching ratios. The penguin amplitudes that do not related to tree amplitudes are either factorizable and estimated in the pole model, or suppressed by the helicity conservation and negligible. More details can be found in Refs. [24, 25]. The penguin amplitudes are enhanced by the nonperturbative-QCD effects in the FAT approach, $\mathcal{P}/\mathcal{T} = \mathcal{O}(1)$, which results in a 10^{-3} order CPV in the D meson decays compared to the naive expectation that $A_{CP}^{\rm charm} \sim \frac{\alpha_s(\mu_c)}{\pi}\frac{|V_{ub}V_{cb}^*|}{|V_{us}V_{cs}^*|} = \mathcal{O}(10^{-4})$.

Precise prediction of the difference of CP asymmetry in the $D^0 \to K^+K^-$ and $D^0 \to \pi^+\pi^-$ modes (known as ΔA_{CP}) is a remarkable achievement of the FAT approach. As early as 2011, the LHCb Collaboration reported the evidence of charm CPV with $\Delta A_{CP} = (-8.2 \pm 2.4) \times 10^{-3}$ [38]. Because of the different understanding of the non-perturbative dynamics in penguin, the theoretical estimation for ΔA_{CP} ranging from 10^{-4} to 10^{-2}. In 2012, the FAT approach predicted that

$$\Delta A_{CP}^{\rm FAT} = (-1.87 \sim -0.57) \times 10^{-3}. \quad (13)$$

It is much smaller than the data in 2011 but consistent with the newest result by the LHCb measurement [2]:

$$\Delta A_{CP}^{\rm EXP} = (-1.54 \pm 0.29) \times 10^{-3}. \quad (14)$$

A comparison between the experimental measurements and the FAT prediction of ΔA_{CP} is shown in Fig. 3. The consistency of experimental result with theoretical prediction indicates reliability of the FAT approach for estimating the penguin amplitudes. Another work that gave a reasonable prediction of ΔA_{CP} in 2012 is Ref. [14],

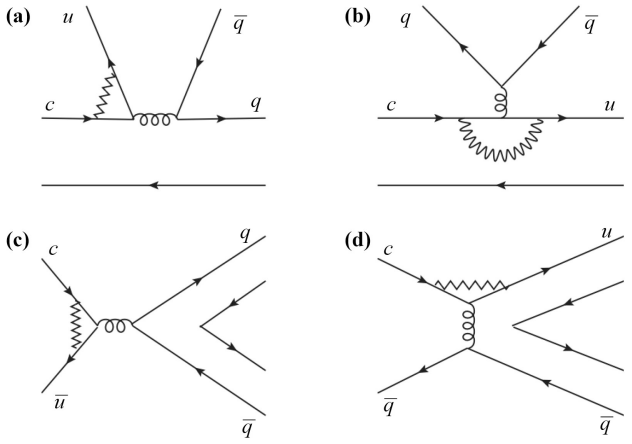

Fig. 2 Topological penguin diagrams contributing to the two-body non-leptonic D decays with **(a)** the color-favored penguin amplitude P, **(b)** the color-suppressed penguin amplitude P_C, **(c)** the gluon-annihilation penguin amplitude P_E, and **(d)** the gluon-exchange penguin amplitude P_A. The diagrams are reproduced from Ref. [25].

in which the penguin-exchange diagram is assumed to be identical to the long-distance contribution to W-exchange diagram, $P_A \simeq E$[2]. ΔA_{CP} is predicted to be $(-1.39 \pm 0.04) \times 10^{-3}$ or $(-1.51 \pm 0.04) \times 10^{-3}$, and updated with similar results in Ref. [39]. A detailed comparison between FAT prediction and the hypothesis of $P_A \simeq E$ was performed in Ref. [39]. And the possible theoretical explanation of $P_A \simeq E$ was given by analyzing the rescattering contribution to penguin diagram in which $(P + P_A)^{LD} \simeq E^{LD}$ is concluded [40]. In fact, the assumptions that $P = E$, $P_A = E$ or $P + P_A = E$ could give similar results because P and P_A always appear as $P + P_A$. Thereby, the CP asymmetry difference in $D^0 \to K^+K^-$ and $D^0 \to \pi^+\pi^-$ can be explained by the interference between tree diagrams $T + E$ with long-distance penguin amplitudes $P + P_A$ through final-state interaction. Although some theorists proposed the beyond SM explanations for the large observed CPV [41–43], we prefer to

[1] The $q\bar{q}$ forms a color-singlet meson in P_C, there should be two and three gluon lines to attach to the pseudoscalar and vector meson, respectively. Notice the notions are different from literature such as [13].

[2] P_A is labeled as P_E in [14].

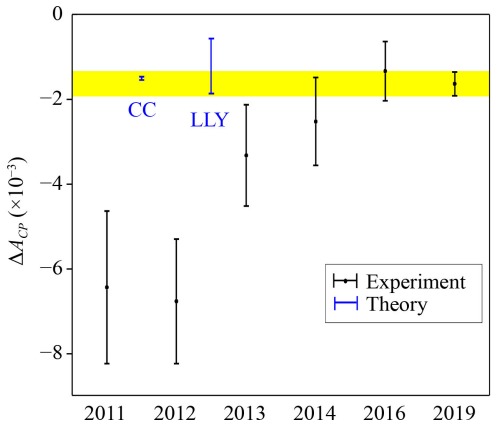

Fig. 3 Comparison of ΔA_{CP} between experimental measurements (in black) and theoretical prediction of the FAT approach (in blue). Experimental results are corresponding to the world-average values for specific year as extracted by the HFLAV [36]. The theoretical results labeled by CC and LLY are taken from Ref. [14] and Ref. [24] respectively. The yellow band is the recent experimental result given by LHCb [2].

believe it comes from the non-perturbative QCD enhancement.

In Refs. [24, 25], the *CP* asymmetries in other D decay channels are calculated in the FAT approach. To compare the FAT predictions with experimental data, we list them in Table 3. Because of the large uncertainties, it is difficult to test the FAT approach with experimental data of individual decay channels at the present stage. More precise experimental observations are looked forward. Besides, the three-body decay $D^+ \to K^+K^-\pi^+$ might be the next potential mode to reveal the *CPV* in charm due to the large branching fraction $\mathcal{B}r(D^+ \to K^+K^-\pi^-) = (9.51 \pm 0.34) \times 10^{-3}$ and the large *CPV* in the two-body decay $D^+ \to K^+\overline{K}_0^*(1430)^0$ according to the FAT approach [44].

Due to the large non-perturbative effects at the charm scale, it is difficult to test new physics in the *CPV* of singly Cabibbo-suppressed D decays. Compared to the singly Cabibbo-suppressed (SCS) case, both the Cabibbo-favored (CF) and doubly Cabibbo-suppressed (DCS) amplitudes are at tree level. The amplitudes extracted from branching fractions in the FAT approach are more reliable in the CF and DCS modes and hence could provide a promising signal of new physics. In Ref. [45], we pointed out a new *CP*-violating effect in charm decays into neutral kaons resulting from the interference between two tree (Cabibbo-favored and doubly Cabibbo-suppressed) amplitudes with the mixing of final-state mesons, namely $A_{CP}^{\rm int}$, and predicted it in the FAT approach. A schematic description of the chain decay $D^+ \to \pi^+K(t)\,(\to \pi^+\pi^-)$ and the time-dependent *CP* asymmetries in this mode as functions of t/τ_S are shown in Fig. 4. It is found the new effect $A_{CP}^{\rm int}$ could reach an order of 10^{-3} or even 10^{-2} in the range of $2\tau_S < t < 5\tau_S$. It is much larger than the direct *CP* asymmetry induced by interference between the Cabibbo-favored and doubly Cabibbo-suppressed amplitudes, $A_{CP}^{\rm dir}$. This discovery corrected the long-standing misunderstanding that only the *CPV* in K^0–$\overline{K}^0$ mixing and the direct *CPV* in charm decay exist in the charm decays into neutral kaons. It is instructive to search for new physics in charm sector. The new effect is accessible in experiments and could be revealed by measuring the difference of the time-dependent *CP* asymmetries in the $D^+ \to \pi^+K_S^0$ and $D^+ \to \pi^+K_S^0$ modes on the LHCb and Belle II.

The FAT approach has also been applied to the studies of K_S^0–K_L^0 asymmetries which induced by interference between the Cabibbo-favored and the doubly Cabibbo-suppressed amplitudes in the D meson decays [48]. The comparison of K_S^0–K_L^0 asymmetries estimated in the FAT approach with experimental data is found in Table 4. The K_S^0–K_L^0 asymmetries in the D^0-meson decays in the FAT approach are shifted by the D^0–$\overline{D}^0$ mixing parameter $y_D \simeq 0.006$ compared with other theoretical results [16, 49, 50]. The data of K_S^0–K_L^0 asymmetries in the $D^0 \to K_{S,L}^0\omega$ and $D^0 \to K_{S,L}^0\phi$ disagree with the FAT predictions. The most possible reason is that the assumption of $E_P = E_V$ in the FAT approach is not satisfied. It can be potentially improved in the FAT approach, which is left for future works.

The FAT approach could also provide us with a glimpse to the charm mixing dynamics because the contributions to D^0–$\overline{D}^0$ mixing from individual intermediate channels can be summed up in an exclusive approach. In Ref. [33], we estimated the D^0–$\overline{D}^0$ mixing parameter y in the FAT approach. Compared to the diagrammatic approach based on the $SU(3)_F$ symmetry [51], the FAT approach provides a more precise treatment

Table 3 Comparison for FAT predictions and experimental data of CP asymmetries in the singly Cabibbo-suppressed charm decays in units of 10^{-3}. Most data are taken from PDG [1].

Channel	FAT	Data	Channel	FAT	Data
$D^0 \to \pi^+\pi^-$	0.58	1.3 ± 1.4	$D^0 \to \pi^0\pi^0$	0.05	-0 ± 6
$D^0 \to K_S^0K_S^0$	1.38	-19 ± 10	$D^0 \to K^+K^-$	−0.42	-0.7 ± 1.1
$D^0 \to \eta\phi$	0.003	-20 ± 40	$D^+ \to \pi^+\pi^0$	0	4 ± 13
$D^+ \to \pi^+\eta$	−0.26	3 ± 8	$D^+ \to \pi^+\eta'$	1.18	-6 ± 7
$D^+ \to \pi^+\phi$	−0.0001	0.1 ± 0.9	$D_s^+ \to K^+\pi^0$	0.39	20 ± 40
$D_s^+ \to K^+\eta$	0.70	18 ± 19	$D_s^+ \to K^+\eta'$	−1.60	60 ± 190

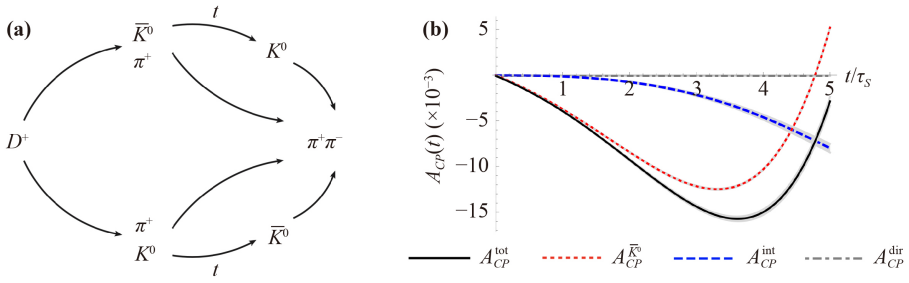

Fig. 4 Schematic description of the chain decay $D^+ \to \pi^+ K(t)\ (\to \pi^+\pi^-)$ **(a)** and time-dependent CP asymmetries as functions of t/τ_S **(b)**. Reproduced from Ref. [45].

Table 4 Comparison of K_S^0–K_L^0 asymmetries estimated in the FAT approach with experimental data.

Channel	FAT	Data	Channel	FAT	Data
$D^0 \to K_{S,L}^0\pi^0$	0.113 ± 0.001	0.108 ± 0.035 [46]	$D^+ \to K_{S,L}^0\pi^+$	0.025 ± 0.008	0.022 ± 0.024 [46]
$D^0 \to K_{S,L}^0\eta$	0.113 ± 0.001	0.080 ± 0.022 [47]	$D^0 \to K_{S,L}^0\eta'$	0.113 ± 0.001	0.080 ± 0.023 [47]
$D^0 \to K_{S,L}^0\omega$	0.113 ± 0.001	-0.024 ± 0.031 [47]	$D^0 \to K_{S,L}^0\phi$	0.113 ± 0.001	-0.001 ± 0.047 [47]

of the $SU(3)$ breaking of strong phases. It is found the contribution from the PP and PV modes is $y_{PP+PV} = (0.21 \pm 0.07)\%$, which is lower than the experimental value $y_{\rm exp} = (0.61 \pm 0.08)\%$ [36] but consistent with the fact that y is generated at second order U-spin breaking [52]. Since the U-spin breaking effects are expected to be more significant in the multi-body D meson decays, they should be included in the evaluation of y. However, it is very difficult to control the $SU(3)_F$ breaking effects in all these modes in an exclusive approach. A new strategy is necessary to understand the charm mixing dynamics in the Standard Model. And treating it as an inverse problem is an attractive attempt [53, 54].

4 Bottom decays

In this section, we shall review the application of the FAT approach in the two-body nonleptonic B mesons decays, including charmed B decays $B \to D^{(*)}P(V)$ [26] and charmless B decays $B \to PP, PV$ [27] and VV [55]. The basis idea of the parametrization for both the tree and penguin amplitudes will be briefly discussed, and some selected results for the branching ratios and CP asymmetries will be presented.

4.1 Two-body charmed B meson decays

The charmed hadronic B decay processes have no contribution from penguin operators. Similar to the D meson decays, four kinds of relevant topologies, T, C, E and A, are involved in the charmed hadronic decays of B mesons. In order to keep the $SU(3)$ breaking effects in the decay amplitudes, we factorize the decay constants and form factors formally from each topological amplitude assisted by factorization hypothesis. And those universal contributions in topological amplitudes are parameterized as some free parameters, χ^C, ϕ^C, χ^E and ϕ^E. With the four fitted parameters from 31 decay modes induced by $b \to c$ transition, we then predicted the branching fractions of 120 decay modes induced though both $b \to c$ and $b \to u$ transitions which can be found in the tables of branching ratios in Ref. [26]. Our results are well consistent with the measured data or to be tested in the LHCb and Belle-II experiments in the future. We found the $SU(3)$ symmetry breaking is more than 10% and even reach 31% at the amplitude level in the FAT approach [26] compared to the conventional $SU(3)_F$ symmetrical topological diagrammatic approach [56]. Besides, the χ^2 fit in the conventional topological diagrammatic approach has to be performed for each category of decays $\overline{B} \to DP$, $\overline{B} \to D^*P$ and $\overline{B} \to DV$ decays due to the large difference between pseudoscalar and vector mesons, resulting in three sets of parameters. With so many parameters, they lost the predictive power of the branching fractions. Even though with much more parameters than in the FAT approach, its χ^2 per degree of freedom ($d.o.f.$) is larger ($\chi^2/d.o.f. = 1.4$ in FAT [26]).

Compared with the QCD-inspired methods [3, 10, 57, 58], the amplitudes of color-suppressed C diagrams are relatively large in the FAT approach where the non-factorizable contribution are dominant, as well as in the topological approach [56]. The hierarchies of topological amplitudes obtained in FAT are [26]

$$\begin{aligned} &|T_c^{DP}| : |C_c^{DP}| : |E_c^{DP}| \sim 1 : 0.45 : 0.1\,, \\ &|T_c^{D^*P}| : |C_c^{D^*P}| : |E_c^{D^*P}| \sim 1 : 0.36 : 0.1\,, \\ &|T_c^{DV}| : |C_c^{DV}| : |E_c^{DV}| \sim 1 : 0.31 : 0.1\,, \end{aligned} \tag{15}$$

which differ from the relation $|T_c^{DP}| \gg |C_c^{DP}| \sim |E_c^{DP}|$ calculated in the PQCD approach [57]. The relatively larger C diagrams have significant impacts on the processes without T diagrams. For example, the topological amplitudes of $\overline{B}^0 \to D^0\rho^0$ and $D^0\omega$ decays are $(E-C)/\sqrt{2}$ and $(E+C)/\sqrt{2}$, respectively. The branching fraction of the $D^0\rho^0$ mode is predicted to be almost one half of that of the $D^0\omega$ mode in the PQCD approach [57], since C and E diagrams contribute destructively for the former mode but constructively for the latter one, which does not agree with the experiment. In the FAT approach, this issue can be explained since both channels are dominated by the C diagram. Another example is $B^+ \to D^{*0}K^+$ mode. Due to the large C diagram, the branching fraction of $B^+ \to D^{*0}K^+$ estimated in the FAT approach is of order of $O(10^{-5})$ [26] compared to $O(10^{-6})$ in the PQCD prediction [58, 59]. Besides, it is easy to see from Eq. (15) that there is non-negligible difference for the C contributions between different category of decays $B \to DP$, $B \to D^*P$ and $B \to DV$.

The relatively large amplitudes of color-suppressed C diagrams in the FAT approach can also used to explain the isospin asymmetry. The $\overline{B} \to D\pi$ system can be decomposed in terms of two isospin amplitudes, $A_{1/2}$ and $A_{3/2}$, which correspond to the transition into $D\pi$ final states with isospin $I = 1/2$ and $I = 3/2$, respectively. The ratio

$$\frac{A_{1/2}}{\sqrt{2}A_{3/2}} = 1 + \mathcal{O}(\Lambda_{\rm QCD}/m_b)\,, \tag{16}$$

is a measure of the departure from the heavy-quark limit [60]. The isospin amplitudes can be expressed by the topological amplitudes as

$$\frac{A_{1/2}}{\sqrt{2}A_{3/2}} = 1 - \frac{3}{2}\left(\frac{C-E}{T+C}\right)\,, \tag{17}$$

and the numerical result in the FAT approach [26] is

$$\left|\frac{A_{1/2}}{\sqrt{2}A_{3/2}}\right|_{D\pi} = 0.65 \pm 0.03, \tag{18}$$

together with relative strong phase between the $I = 3/2$ and $I = 1/2$ amplitudes,

$$\cos\delta = 0.90 \pm 0.04. \tag{19}$$

Comparing with Eq. (16), we observe that the isospin-amplitude ratio shows significant deviation from the heavy-quark limit. Because the contribution from annihilations has been neglected, we can trace this feature back to the large color-suppressed C topologies.

4.2 Two-body charmless B meson decays $B \to PP, PV$

Different from two-body charmed B meson decays with only tree diagrams, charmless B meson decays also receive contributions from penguin diagrams enhanced by CKM matrix elements. Specifically, corresponding to 4-types of tree diagrams, four types of one loop penguin diagrams grouped into QCD penguin and electro-weak penguin (EW penguin) topologies should be added. Ignoring some small diagrams, only five penguin diagrams are kept: color-favored QCD penguin emission diagram P, color-suppressed QCD penguin emission diagram P_C, W-annihilation penguin diagram P_A, the W penguin exchange diagram P_E and electro-weak penguin emission diagram P_{EW}, as shown in Fig. 5.

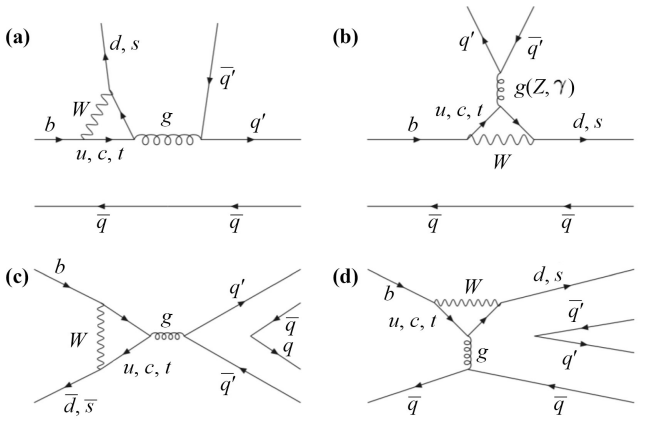

Fig. 5 Topological penguin diagrams contributing to $B \to PP$ and $B \to PV$ decays: **(a)** the color-favored QCD-penguin diagram, P; **(b)** the flavor-singlet QCD-penguin diagram, P_C and EW-penguin diagram P_{EW}; **(c)** the exchange type QCD-penguin diagram, P_E and **(d)** the QCD-penguin annihilation diagram, P_A. The diagrams are reproduced from Ref. [26].

Similar to the case of the charmed B decays, the non-perturbative contributions of tree diagrams are parameterized as universal magnitudes (χ) and phases (ϕ). However, we can not fit three types of charmless B decay amplitude categories $B \to PP$, $B \to PV$ (P emission) and $B \to VP$ (V emission) together. For emission diagrams C, the case of the pseudo-scalar emission is different from case of the vector emission. We hence parameterize the C diagram magnitude and associated phase as $\chi^C e^{i\phi^C}$ in $B \to PP$, VP decays and $\chi^{C'} e^{i\phi^{C'}}$ in $B \to PV$, respectively, to distinguish cases in which the emitted meson is pseudo-scalar or vector. In terms of QCD penguin amplitude, we consider all contributions from every topological diagram in Fig. 5, where topology P contributes most. The leading contribution from topology P diagram is similar to the color favored tree diagram T and predicted from QCD calculations in all the three types of $B \to PP$, $B \to VP$ and $B \to PV$ categories. Since the chiral enhancement only contributes to the pseudo-scalar meson (Goldstone boson) emission diagram, we include it only in $B \to PP$ and $B \to VP$ categories by introducing two parameters χ^P, ϕ^P. In the flavor-singlet QCD penguin diagram P_C, we distinguish

Table 5 The amplitudes and strong phases of topological diagrams in the FAT approach [26] corresponding to contributions in the QCDF [5]. The topology A and P_E are neglected in the FAT approach. The electroweak penguin contributions of $\alpha_4^{\rm EW}$, $\beta_3^{\rm EW}$ and $\beta_4^{\rm EW}$ in the QCDF are also neglected in the FAT approach.

Diagram	T	C	P_C	$P(PP)$	$P_{\rm EW}$	E	A	$P_A(PV)$	P_E
FAT	a_1	$\chi^{C^{(\prime)}}\mathrm{e}^{\mathrm{i}\phi^{C^{(\prime)}}}$	$\chi^{P_C^{(\prime)}}\mathrm{e}^{\mathrm{i}\phi^{P_C^{(\prime)}}}$	$a_4(\mu)+\chi^P\mathrm{e}^{\mathrm{i}\phi^P}r_\chi$	$a_9(\mu)$	$\chi^E\mathrm{e}^{\mathrm{i}\phi^E}$	–	$-\mathrm{i}\chi^{P_A}\mathrm{e}^{\mathrm{i}\phi^{P_A}}$	–
	–	$0.48\mathrm{e}^{-1.58\mathrm{i}}$	$0.048\mathrm{e}^{1.56\mathrm{i}}$	$-0.12\mathrm{e}^{-0.24\mathrm{i}}$	–0.009	$0.057\mathrm{e}^{2.71\mathrm{i}}$		$0.0059\mathrm{e}^{-0.006\mathrm{i}}$	
QCDF	α_1	α_2	α_3	α_4	$\alpha_3^{\rm EW}$	β_1	β_2	β_3	β_4
	–	$0.22\mathrm{e}^{-0.53\mathrm{i}}$	$0.011\mathrm{e}^{2.23\mathrm{i}}$	$-0.089\mathrm{e}^{0.11\mathrm{i}}$	$-0.009\mathrm{e}^{0.04\mathrm{i}}$	0.025	–0.011	–0.008	–0.003

them as χ^{P_C}, ϕ^{P_C} for $B\to PP$ and $B\to VP$ decays and $\chi^{P'_C}$, $\phi^{P'_C}$ for $B\to PV$ decays, respectively. The penguin annihilation diagram P_A is not distinguishable in weak interaction from the diagram P, we include the non-perturbative contributions of P_A diagram in the parameter χ^P, ϕ^P in the $B\to PP$ and $B\to VP$ modes. While, for $B\to PV$ decay, we introduce two parameters χ^{P_A}, $\mathrm{e}^{\mathrm{i}\phi^{P_A}}$ for penguin annihilation diagram P_A. The contribution from P_E is expected to be smaller than P_A and negligible. For EW-penguin diagrams, we only keep the largest contribution diagram from EW-penguin contributions, P_{EW}. Similar to the T diagram, we evaluate P_{EW} without introducing new parameters.

The number of free parameters in the FAT approach is significantly reduced from the previous topological diagram approach [19]. We fit 14 parameters from 37 experimental measured branching fractions and 11 CP asymmetry parameters of $B\to PP$ and $B\to PV$ decays, with much smaller χ^2 per degree of freedom ($\chi^2/d.o.f=1.3$ in the FAT approach) than in previous topological diagram approach [19]. The mapping of these topologies to well-known QCDF amplitudes introduced in [4, 5] is shown in Table 5. It is apparent that there are huge differences between numbers fitted from experimental data in the FAT and the calculated results in the QCDF [5], especially for the strong phases. That might be the reason why the current QCDF and SCET calculation can predict the branching ratios but can not explain the direct CP asymmetries well. Apart form QCD corrections [61–69], power corrections in QCD calculations [70–78] and also QED corrections [79, 80] might be crucial to solve such problems.

We list the direct CP asymmetries ($\mathcal{A}$) and mixing-induced CP asymmetries ($\mathcal{S}$) of $\overline{B}\to PP$ decays in Table 6, with the addition of the results from conventional flavor diagram approach [19] for comparison. The $B^-\to\pi^0K^-$ decay is naively expected to have the same dominant decay amplitude T and P as $\overline{B}^0\to\pi^+K^-$ decay, and thus one expects similar direct CP asymmetries [81]. However, experimentally these two direct CP asymmetries are quite different, even with an opposite sign. That is the so-called πK CP-puzzle. From the Table 5, we know the large C contribution with large strong phase can resolve the so called πK puzzle. However, only a large C magnitude can not explain another puzzle, the $\pi\pi$ puzzle: theoretically $\mathcal{B}(B^0\to\pi^0\pi^0)<\mathcal{B}(B^0\to\pi^0\rho^0)<\mathcal{B}(B^0\to\rho^0\rho^0)$, but experimentally they are in the inverse order. In the FAT approach, the $\pi\pi$ puzzle can be resolved by different strong phase ϕ^C and $\phi^{C'}$ representing the pseudo-scalar and vector meson emission, respectively, even though χ^C and $\chi^{C'}$ are in similar size [26]:

$$\chi^C=0.48\pm0.06,\quad \phi^C=-1.58\pm0.08,$$
$$\chi^{C'}=0.42\pm0.16,\quad \phi^{C'}=1.59\pm0.17\,. \tag{20}$$

The difference in strong phase is also agreement with the Glauber phase factor [29], associated with the Goldstone boson π, to resolve the $B\to\pi\pi$, $B\to\pi\rho$ and $B\to\rho\rho$ puzzles consistently.

4.3 B decays with two vector meson $B\to VV$

The vector mesons can be produced in three polarization states, corresponding to the longitudinal L and two helicity ±1 states. So the decay amplitudes can be described with definite final state helicity $\mathcal{A}_{L,\pm}$. These decays have rich polarization observables, apart from decay widths and CP asymmetries in contrast to the $PP(PV)$ final states. Theoretically, the longitudinal polarisation amplitude $\mathcal{A}_L$ is similar to the decay in PP, PV final states. Then we have 8 unknown real parameters to be fitted for $\mathcal{A}_L$. For the transverse amplitudes, it is convenient to use the linear polarised form $\mathcal{A}_{/\!/}=(\mathcal{A}^++\mathcal{A}^-)/\sqrt{2}$, $\mathcal{A}_\perp=(\mathcal{A}^+-\mathcal{A}^-)/\sqrt{2}$. The transverse amplitudes are power suppressed relative to longitudinal amplitude. So the endpoint divergences of transverse amplitudes emerge even at leading power in QCDF [82], which decreases the predictive power. In the FAT approach, besides the color-favored tree diagram T and QCD-penguin diagram P which do not introduce any parameter, we only consider the penguin annihilation diagram P_A. Thus, there are only 10 universal parameters totally, which will be fitted by experimental data. The best-fitted values of the parameters are given in Ref. [83].

Because of the V–A coupling of weak interaction, a specific pattern of the three helicity amplitudes is naively expected [84]:

$$\bar{\mathcal{A}}^0:\bar{\mathcal{A}}^-:\bar{\mathcal{A}}^+=1:\frac{\Lambda_{QCD}}{m_b}:\left(\frac{\Lambda_{QCD}}{m_b}\right)^2, \tag{21}$$

for $\overline{B}$ meson. For B meson, we exchange the superscript

Table 6 The direct CP asymmetries ($\mathcal{A}$) and mixing-induced CP asymmetries ($\mathcal{S}$) of $\overline{B} \to PP$ decays predicted by the FAT approach [26] compared to data [1] and the results from the conventional flavor diagram approach [19].

Mode	$\mathcal{A}_{\rm exp}$	$\mathcal{A}_{\rm FAT}$	$\mathcal{A}_{\rm Flavor\ diagram}$	$\mathcal{S}_{\rm exp}$	$\mathcal{S}_{\rm FAT}$	$\mathcal{S}_{\rm Flavor\ diagram}$
$\pi^+\pi^-$	0.32 ± 0.04	0.31 ± 0.04	0.326 ± 0.081	-0.65 ± 0.04	-0.60 ± 0.03	-0.717 ± 0.061
$\pi^0\pi^0$	0.33 ± 0.22	0.57 ± 0.06	0.611 ± 0.113		0.58 ± 0.06	0.454 ± 0.112
$\pi^0\eta$		-0.16 ± 0.16	0.566 ± 0.114		-0.98 ± 0.04	-0.098 ± 0.338
$\pi^0\eta'$		0.39 ± 0.14	0.385 ± 0.114		-0.90 ± 0.07	0.142 ± 0.234
$\eta\eta$		-0.85 ± 0.06	-0.405 ± 0.129		0.33 ± 0.12	-0.796 ± 0.077
$\eta\eta'$		-0.97 ± 0.04	-0.394 ± 0.117		-0.20 ± 0.15	-0.903 ± 0.049
$\eta'\eta'$		-0.87 ± 0.07	-0.122 ± 0.136		-0.46 ± 0.14	-0.964 ± 0.037
$\pi^0 K_s$	0.00 ± 0.13	-0.14 ± 0.03	-0.173 ± 0.019	0.58 ± 0.17	0.73 ± 0.01	0.754 ± 0.014
ηK_s		-0.30 ± 0.10	-0.301 ± 0.041		0.68 ± 0.04	0.592 ± 0.035
$\eta' K_s$	0.06 ± 0.04	0.030 ± 0.004	0.022 ± 0.006	0.63 ± 0.06	0.69 ± 0.00	0.685 ± 0.004
$K^0\bar{K}^0$		-0.057 ± 0.002	0.017 ± 0.041	0.8 ± 0.5	0.099 ± 0.002	0
$\pi^-\pi^0$	0.03 ± 0.04	-0.026 ± 0.003	0.069 ± 0.027			
$\pi^-\eta$	-0.14 ± 0.07	-0.14 ± 0.07	-0.081 ± 0.074			
$\pi^-\eta'$	0.06 ± 0.16	0.37 ± 0.07	0.374 ± 0.087			
$\pi^-\bar{K}^0$	-0.017 ± 0.016	0.0027 ± 0.0001	0			
$\pi^0 K^-$	0.037 ± 0.021	0.065 ± 0.024	0.047 ± 0.025			
ηK^-	-0.37 ± 0.08	-0.22 ± 0.08	-0.426 ± 0.043			
$\eta' K^-$	0.04 ± 0.011	-0.021 ± 0.007	-0.027 ± 0.008			
K^-K^0	-0.21 ± 0.14	-0.057 ± 0.002	0			
π^+K^-	-0.083 ± 0.004	-0.081 ± 0.005	-0.080 ± 0.011			

Table 7 Comparison of the FAT approach [83] and the experimental results [1] for observables of $B^- \to \rho^-\rho^0$, $\overline{B}^0 \to \rho^+\rho^-$ and $\overline{B}^0 \to \rho^0\rho^0$.

Mode	$\mathcal{B}$ (10^{-6})	f_L (%)	$f_\perp$ (%)	$\phi_{//}$ (rad)	$\phi_\perp$ (rad)
$B^- \to \rho^-\rho^0$	21.7 ± 5.1	95.5 ± 1.5	2.22 ± 0.64	-0.09 ± 0.05	-0.09 ± 0.05
Expt.	24.0 ± 1.9	95 ± 1.6			
$\overline{B}^0 \to \rho^+\rho^-$	29.5 ± 6.5	92.6 ± 1.6	3.65 ± 0.91	-0.27 ± 0.08	-0.27 ± 0.08
Expt.	27.7 ± 1.9	$99.0^{+2.1}_{-1.9}$			
$\overline{B}^0 \to \rho^0\rho^0$	0.94 ± 0.49	81.7 ± 10.8	9.21 ± 5.50	-0.04 ± 0.44	-0.03 ± 0.44
Expt.	0.96 ± 0.15	71^{+8}_{-9}			
	A_{CP} (%)	A^0_{CP} (%)	$A^\perp_{CP}$ (%)	$\Delta\phi_{//}$ (rad)	$\Delta\phi_\perp$ (rad)
$B^- \to \phi K^{*-}$	0	0	0	0	0
Expt.	-5 ± 5				
$\overline{B}^0 \to \phi\overline{K}^{*0}$	-8.10 ± 2.94	1.30 ± 0.54	-16.3 ± 8.2	-0.41 ± 0.05	-0.41 ± 0.05
$\overline{B}^0_s \to \phi\phi$	49.7 ± 13.4	10.5 ± 9.6	-46.9 ± 13.9	1.89 ± 0.19	1.89 ± 0.19

– and +. The amplitudes of tree dominated decays respect the hierarchy (21), and f_L are closed to 1. Taking the three $B \to \rho\rho$ decay modes in Table 7 as an example, we list the numerical results of longitudinal polarization for each topological diagram of these decays,

$$|T^{B\to\rho_L\rho_L}| : |C^{B\to\rho_L\rho_L}| : |E^{B\to\rho_L\rho_L}| : |P^{B\to\rho_L\rho_L}| : |P_A^{B\to\rho_L\rho_L}| = 1 : 0.22 : 0.21 : 0.14 : 0.08. \quad (22)$$

For the decay $B^- \to \rho^-\rho^0$, although the absolute value of the C diagram is suppressed, it can enhance the magnitude of the decay amplitude by 20%. With the larger contribution from C diagram, the large branching fraction of $\overline{B}^0 \to \rho^0\rho^0$ is also explained.

However, large transverse polarization fractions ($\sim 50\%$) of $B \to \phi K^*$ have been measured by Babar [85] and Belle [86] in 2003. Later on, some other penguin-dominated decays, such as $B \to \rho K^*$ and $B_s \to \phi\phi$, have also been found with large transverse polarization fractions. As mentioned before, we use the P_A diagram to explain these large transverse polarization fraction. In Table 8, we list the results of three best measured channels

Table 8 Comparison of the FAT approach [83] and the experimental results [1] for observables of $B^- \to \phi K^{*-}$, $\overline{B}^0 \to \phi \overline{K}^{*0}$ and $\overline{B}_s^0 \to \phi\phi$.

Mode	$\mathcal{B}$ (10^{-6})	f_L (%)	$f_\perp$ (%)	$\phi_{//}$ (rad)	$\phi_\perp$ (rad)
$B^- \to \phi K^{*-}$	9.31 ± 2.81	48.0 ± 16.0	25.9 ± 8.6	2.47 ± 0.27	2.47 ± 0.27
Expt.	10 ± 2	50 ± 5	20 ± 5	2.34 ± 0.18	2.58 ± 0.17
$\overline{B}^0 \to \phi \overline{K}^{*0}$	8.64 ± 2.61	48.0 ± 16.0	26.0 ± 8.6	2.47 ± 0.27	2.47 ± 0.27
Expt.	10.0 ± 0.5	49.7 ± 1.7	22.4 ± 1.5	2.43 ± 0.11	2.53 ± 0.09
$\overline{B}_s^0 \to \phi\phi$	26.4 ± 7.6	39.7 ± 16.0	31.2 ± 8.9	2.53 ± 0.28	2.56 ± 0.27
Expt.	18.7 ± 1.5	37.8 ± 1.3	29.2 ± 0.9	2.56 ± 0.06	2.818 ± 0.192
	A_{CP} (%)	A_{CP}^0 (%)	$A_{CP}^\perp$ (%)	$\Delta\phi_{//}$ (rad)	$\Delta\phi_\perp$ (rad)
$B^- \to \phi K^{*-}$	1.00 ± 0.27	1.26 ± 0.71	-1.16 ± 0.30	-0.02 ± 0.00	-0.02 ± 0.00
Expt.	-1 ± 8	17 ± 11	22 ± 25	0.07 ± 0.21	0.19 ± 0.21
$\overline{B}^0 \to \phi \overline{K}^{*0}$	1.00 ± 0.27	1.26 ± 0.71	-1.16 ± 0.30	-0.02 ± 0.00	-0.02 ± 0.00
Expt.	0 ± 4	-0.7 ± 3.0	-2 ± 6	0.05 ± 0.05	0.08 ± 0.05
$\overline{B}_s^0 \to \phi\phi$	0.83 ± 0.28	1.55 ± 0.85	-1.02 ± 0.29	-0.01 ± 0.00	-0.01 ± 0.00

$B^- \to \phi K^{*-}$, $\overline{B}^0 \to \phi \overline{K}^{*0}$ and $\overline{B}_s^0 \to \phi\phi$ as an illustration. In these decays, the magnitudes of QCD penguin diagram P, P_c, and P_A are at the same order. For $\overline{B}_s^0 \to \phi\phi$ decay, our center value is a bit larger than the experimental data, and the predicted polarization fractions are in agreement with the data. The acceptable divergency is in fact constrained by the measured branching ratio of $\overline{B}_s^0 \to \phi K^{*0}$ decay.

5 Summary and outlook

The FAT approach is a data driven framework to study heavy meson decays. Compared to QCD calculations, it gets a better chance to be consistent with data, if all crucial dynamics are figured out and parameterized in a proper way. It is useful in two aspects, one experimentally and the other one theoretically. From the experimental point of view, it can make trustworthy predictions for unmeasured observables, e.g., D/B meson decay branching ratios and also CP asymmetries, which will help the discovery of new decay channels and new CP violation effects in experiments. One highlight is the prediction for ΔA_{CP} confirmed by later LHCb measurement, which was also the first direct CP violation discovery in the charm sector. From the theoretical point of view, the amplitude structures of the decay processes can be decoded in the FAT approach, which will provide hints for the directions of future theoretical studies. For example, the understanding of the large magnitude and large strong phase in the C amplitude in B decays require more theoretical efforts.

In the end, it is important to clarify that the FAT approach should not refer to any of the parametrization schemes that has appeared in any of the existing papers [24–27]. Apparently, the parametrization schemes for D and B decays are quite different from each other. Instead, it should be regarded as a more general framework, in which the short distance dynamics and the long distance dynamics of different topological amplitudes are factorized with the former formulated by corresponding Wilson coefficients and the latter as hadronic matrix elements either calculable or parameterized. In the parametrization, important $SU(3)$ breaking effects are expected to be figured out, which leads to some arbitrariness and also leaves space to improve.

Until now, although the FAT approach has made many remarkable achievements, it still awaits more efforts in the future to improve the parametrization schemes for both the D and B decays, especially in such a stage with more and more precise data. For example, the FAT approach cannot explain the branching fractions of some $D \to PV$ modes (such as $D_s^+ \to \eta'\rho^+$ and $D^0 \to \eta\overline{K}^{*0}$) very well. The newest measurements of K_S^0–K_L^0 asymmetries indicating the assumption of $E_V = E_P$ and $A_V = A_P$ in the FAT should be modified to match experimental data. These questions should be solved in the future. Besides, the FAT approach is expected to be applied to more decay modes such as $D \to VV$ and heavy baryon decays.

Declarations The authors declare that they have no competing interests and there are no conflicts.

Acknowledgements The authors would like to thank Professors Xin Liu, Zhen-Jun Xiao & Ruilin Zhu for the invitation to write a review article on the factorization-assisted topological-amplitude approach. The authors are grateful to Hsiang-Nan Li, Cai-Dian Lü and Fu-Sheng Yu for original works in innovating the FAT approach. This work was supported by the National Natural Science Foundation of China (Grant Nos. 12005068, 12105148, 12105112, and 12105099) and the Natural Science Foundation of Jiangsu Education Committee (Grant No. 21KJB140027). A preprint has previously been published [87].

References

1. R. L. Workman, et al. [Particle Data Group], Review of Particle Physics, *Prog. Theor. Exp. Phys.* 2022, 083C01 (2022)
2. R. Aaij, et al. [LHCb], Observation of *CP* violation in charm decays, *Phys. Rev. Lett.* 122(21), 211803 (2019)
3. M. Beneke, G. Buchalla, M. Neubert, and C. T. Sachrajda, QCD factorization for $B \to \pi\pi$ decays: Strong phases and *CP* violation in the heavy quark limit, *Phys. Rev. Lett.* 83(10), 1914 (1999), arXiv: hep-ph/9905312
4. M. Beneke and M. Neubert, QCD factorization for $B \to PP$ and $B \to PV$ decays, *Nucl. Phys. B* 675(1–2), 333 (2003), arXiv: hep-ph/0308039
5. M. Beneke, G. Buchalla, M. Neubert, and C. T. Sachrajda, QCD factorization in $B \to \pi K, \pi\pi$ decays and extraction of Wolfenstein parameters, *Nucl. Phys. B* 606(1–2), 245 (2001), arXiv: hep-ph/0104110
6. Y. Y. Keum, H. N. Li, and A. I. Sanda, Fat penguins and imaginary penguins in perturbative QCD, *Phys. Lett. B* 504(1–2), 6 (2001), arXiv: hep-ph/0004004
7. Y. Y. Keum, H. N. Li, and A. I. Sanda, Penguin enhancement and $B \to K\pi$ decays in perturbative QCD, *Phys. Rev. D* 63(5), 054008 (2001), arXiv: hep-ph/0004173
8. C. D. Lü, K. Ukai, and M. Z. Yang, Branching ratio and *CP* violation of $B \to \pi\pi$ decays in the perturbative QCD approach, *Phys. Rev. D* 63(7), 074009 (2001), arXiv: hep-ph/0004213
9. C. D. Lü and M. Z. Yang, $B \to \pi\rho, \pi\omega$ decays in perturbative QCD approach, *Eur. Phys. J. C* 23(2), 275 (2002), arXiv: hep-ph/0011238
10. C. W. Bauer, D. Pirjol, and I. W. Stewart, Proof of factorization for $B \to D\pi$, *Phys. Rev. Lett.* 87(20), 201806 (2001), arXiv: hep-ph/0107002
11. C. W. Bauer, D. Pirjol and I. W. Stewart, Soft-collinear factorization in effective field theory, *Phys. Rev. D* 65, 054022 (2002), arXiv: hep-ph/0109045
12. M. Beneke, A. P. Chapovsky, M. Diehl, and T. Feldmann, Soft-collinear effective theory and heavy-to-light currents beyond leading power, *Nucl. Phys. B* 643(1–3), 431 (2002), arXiv: hep-ph/0206152
13. H. Y. Cheng and S. Oh, Flavor $SU(3)$ symmetry and QCD factorization in $B \to PP$ and PV decays, *J. High Energy Phys.* 09, 024 (2011), arXiv: 1104.4144 [hep-ph]
14. H. Y. Cheng and C. W. Chiang, $SU(3)$ symmetry breaking and *CP* violation in $D \to PP$ decays, *Phys. Rev. D* 86(1), 014014 (2012)
15. H. Y. Cheng and C. W. Chiang, Direct *CP* violation in two-body hadronic charmed meson decays, *Phys. Rev. D* 85, 034036 (2012), arXiv: 1201.0785 [hep-ph] [Erratum: *Phys. Rev. D* 85, 079903 (2012)]
16. H. Y. Cheng and C. W. Chiang, Two-body hadronic charmed meson decays, *Phys. Rev. D* 81(7), 074021 (2010)
17. L. L. Chau and H. Y. Cheng, Analysis of two-body decays of charm mesons using the quark-diagram scheme, *Phys. Rev. D* 36(1), 137 (1987)
18. L. L. Chau and H. Y. Cheng, Quark-diagram analysis of two-body charm decays, *Phys. Rev. Lett.* 56(16), 1655 (1986)
19. H. Y. Cheng, C. W. Chiang, and A. L. Kuo, Updating $B \to PP$, VP decays in the framework of flavor symmetry, *Phys. Rev. D* 91(1), 014011 (2015)
20. L. L. Chau, H. Y. Cheng, W. K. Sze, H. Yao, and B. Tseng, Charmless nonleptonic rare decays of B mesons, *Phys. Rev. D* 43(7), 2176 (1991) [erratum: *Phys. Rev. D* 58, 019902 (1998)]
21. H. Y. Cheng, C. W. Chiang, and A. L. Kuo, Global analysis of two-body $D \to VP$ decays within the framework of flavor symmetry, *Phys. Rev. D* 93(11), 114010 (2016)
22. T. Huber and G. Tetlalmatzi-Xolocotzi, Estimating QCD-factorization amplitudes through $SU(3)$ symmetry in $B \to PP$ decays, *Eur. Phys. J. C* 82(3), 210 (2022)
23. S. Müller, U. Nierste, and S. Schacht, Topological amplitudes in D decays to two pseudoscalars: A global analysis with linear $SU(3)_F$ breaking, *Phys. Rev. D* 92(1), 014004 (2015)
24. H. Li, C. D. Lu, and F. S. Yu, Branching ratios and direct *CP* asymmetries in $D \to PP$ decays, *Phys. Rev. D* 86(3), 036012 (2012)
25. Q. Qin, H. Li, C. D. Lü, and F. S. Yu, Branching ratios and direct *CP* asymmetries in $D \to PV$ decays, *Phys. Rev. D* 89(5), 054006 (2014)
26. S. H. Zhou, Y. B. Wei, Q. Qin, Y. Li, F. S. Yu, and C. D. Lu, Analysis of two-body charmed B meson decays in factorization-assisted topological-amplitude approach, *Phys. Rev. D* 92(9), 094016 (2015)
27. S. H. Zhou, Q. A. Zhang, W. R. Lyu, and C. D. Lü, Analysis of charmless two-body B decays in factorization-assisted topological-amplitude approach, *Eur. Phys. J. C* 77(2), 125 (2017)
28. H. Li, Glauber gluons in annihilation amplitudes for heavy meson decays, *Chin. J. Phys.* 73, 649 (2021)
29. H. Li and S. Mishima, Glauber gluons in spectator amplitudes for $B \to \pi M$ decays, *Phys. Rev. D* 90(7), 074018 (2014)
30. J. Beringer, et al. [Particle Data Group], Review of particle physics, *Phys. Rev. D* 86(1), 010001 (2012)
31. P. U. E. Onyisi, et al. [CLEO], Improved measurement of absolute hadronic branching fractions of the D_s^+ meson, *Phys. Rev. D* 88(3), 032009 (2013)
32. M. Ablikim, et al. [BESIII], Measurement of the branching fractions of $D_s^+ \to \eta' X$ and $D_s^+ \to \eta' \rho^+$ in $e^+e^- \to D_s^+ D_s^-$, *Phys. Lett. B* 750, 466 (2015)
33. H. Y. Jiang, F. S. Yu, Q. Qin, H. Li, and C. D. Lü, D^0–$\bar{D}^0$ mixing parameter y in the factorization-assisted topological-amplitude approach, *Chin. Phys. C* 42(6), 063101 (2018)
34. M. Ablikim, et al. [BESIII], Measurements of absolute branching fractions for D mesons decays into two pseudoscalar mesons, *Phys. Rev. D* 97(7), 072004 (2018)
35. Y. Guan, et al. [Belle], Measurement of branching fractions and *CP* asymmetries for $D_s^+ \to K^+ (\eta, \pi^0)$ and $D_s^+ \to \pi^+ (\eta, \pi^0)$ decays at Belle, *Phys. Rev. D* 103(11), 112005 (2021)
36. Y. S. Amhis, et al. [HFLAV], Averages of b-hadron, c-hadron, and τ-lepton properties as of 2018, *Eur. Phys. J. C* 81(3), 226 (2021)
37. M. Saur and F. S. Yu, Charm *CPV*: Observation and prospects, *Sci. Bull. (Beijing)* 65(17), 1428 (2020)

38. R. Aaij, et al. [LHCb], Evidence for *CP* violation in time-integrated $D^0 \to h^-h^+$ decay rates, *Phys. Rev. Lett.* 108(11), 111602 (2012)
39. H. Y. Cheng and C. W. Chiang, Revisiting *CP* violation in $D \to PP$ and VP decays, *Phys. Rev. D* 100(9), 093002 (2019)
40. D. Wang, From topological amplitude to rescattering dynamics, *J. High Energy Phys.* 2022(3), 155 (2022)
41. M. Chala, A. Lenz, A. V. Rusov, and J. Scholtz, ΔA_{CP} within the Standard Model and beyond, *J. High Energy Phys.* 2019(7), 161 (2019)
42. A. Dery and Y. Nir, Implications of the LHCb discovery of *CP* violation in charm decays, *J. High Energy Phys.* 2019(12), 104 (2019)
43. L. Calibbi, T. Li, Y. Li, and B. Zhu, Simple model for large *CP* violation in charm decays, *B*-physics anomalies, muon g-2, and dark matter, *J. High Energy Phys.* 10, 070 (2020), arXiv: 1912.02676 [hep-ph]
44. H. N. Li, C. D. Lü, and F. S. Yu, Implications on the first observation of charm *CPV* at LHCb, arXiv: 1903.10638 [hep-ph] (2019)
45. D. Wang, F. S. Yu, and H. N. Li, *CP* asymmetries in charm decays into neutral kaons, *Phys. Rev. Lett.* 119(18), 181802 (2017)
46. Q. He, et al. [CLEO], Comparison of $D \to K^0_S\pi$ and $D \to K^0_L\pi$ decay rates, *Phys. Rev. Lett.* 100(9), 091801 (2008)
47. M. Ablikim, et al. [BESIII], Measurements of absolute branching fractions of $D^0 \to K^0_L\phi, K^0_L\eta, K^0_L\omega$, and $K^0_L\eta'$, *Phys. Rev. D* 105(9), 092010 (2022)
48. D. Wang, F. S. Yu, P. F. Guo, and H. Y. Jiang, K^0_S–K^0_L asymmetries in *D*-meson decays, *Phys. Rev. D* 95(7), 073007 (2017)
49. B. Bhattacharya and J. L. Rosner, Charmed meson decays to two pseudoscalars, *Phys. Rev. D* 81(1), 014026 (2010)
50. D. N. Gao, Asymmetries from the interference between Cabibbo-favored and doubly-Cabibbo-suppressed *D* meson decays, *Phys. Rev. D* 91(1), 014019 (2015)
51. H. Y. Cheng and C. W. Chiang, Long-distance contributions to D^0–$\bar{D}^0$ mixing parameters, *Phys. Rev. D* 81(11), 114020 (2010)
52. M. Gronau and J. L. Rosner, Revisiting D^0–$\bar{D}^0$ mixing using *U*-spin, *Phys. Rev. D* 86(11), 114029 (2012)
53. H. N. Li, H. Umeeda, F. Xu, and F. S. Yu, *D* meson mixing as an inverse problem, *Phys. Lett. B* 810, 135802 (2020)
54. H. Li, Dispersive analysis of neutral meson mixing, *Phys. Rev. D* 107(5), 054023 (2023)
55. C. Wang, S. H. Zhou, Y. Li, and C. D. Lu, Global analysis of charmless *B* decays into two vector mesons in soft-collinear effective theory, *Phys. Rev. D* 96(7), 073004 (2017)
56. C. W. Chiang and E. Senaha, Updated analysis of two-body charmed *B* meson decays, *Phys. Rev. D* 75(7), 074021 (2007), arXiv: hep-ph/0702007
57. R. H. Li, C. D. Lu, and H. Zou, $B\,(B_s) \to D_{(s)}P, D_{(s)}V, D^*_{(s)}P$, and $D^*_{(s)}V$ decays in the perturbative QCD approach, *Phys. Rev. D* 78(1), 014018 (2008)
58. H. Zou, R. H. Li, X. X. Wang, and C. D. Lu, The CKM suppressed $B\,(B_s) \to \bar{D}_{(s)}P, \bar{D}_{(s)}V, \bar{D}^*_{(s)}P, \bar{D}^*_{(s)}V$ decays in the perturbative QCD approach, *J. Phys. G* 37(1), 015002 (2010)
59. J. Chai, S. Cheng, and W. F. Wang, Role of D^*_s and their contributions in $B_s \to D_s\, hh'$ decays, *Phys. Rev. D* 103(9), 096016 (2021)
60. M. Beneke and T. Feldmann, Symmetry-breaking corrections to heavy-to-light *B* meson form factors at large recoil, *Nucl. Phys. B* 592(1–2), 3 (2001), arXiv: hep-ph/0008255
61. T. Huber and S. Kränkl, Two-loop master integrals for non-leptonic heavy-to-heavy decays, *J. High Energy Phys.* 2015(4), 140 (2015)
62. G. Bell, M. Beneke, T. Huber, and X. Q. Li, Two-loop current–current operator contribution to the non-leptonic QCD penguin amplitude, *Phys. Lett. B* 750, 348 (2015)
63. T. Huber, S. Kränkl, and X. Q. Li, Two-body non-leptonic heavy-to-heavy decays at NNLO in QCD factorization, *J. High Energy Phys.* 2016(9), 112 (2016)
64. T. Huber, J. Virto, and K. K. Vos, Three-body non-leptonic heavy-to-heavy *B* decays at NNLO in QCD, *J. High Energy Phys.* 2020(11), 103 (2020)
65. G. Bell, M. Beneke, T. Huber, and X. Q. Li, Two-loop non-leptonic penguin amplitude in QCD factorization, *J. High Energy Phys.* 2020, 55 (2020), arXiv: 2002.03262 [hep-ph]
66. H. Li, Y. L. Shen, and Y. M. Wang, Next-to-leading-order corrections to $B \to \pi$ form factors in k_T factorization, *Phys. Rev. D* 85(7), 074004 (2012)
67. S. Cheng, Y. Y. Fan, X. Yu, C. D. Lü, and Z. J. Xiao, NLO twist-3 contributions to $B \to \pi$ form factors in k_T factorization, *Phys. Rev. D* 89(9), 094004 (2014)
68. S. Cheng and Z. J. Xiao, Time-like pion electromagnetic form factors in k_T factorization with the next-to-leading-order twist-3 contribution, *Phys. Lett. B* 749, 1 (2015)
69. S. Cheng and Q. Qin, $Z \to \pi^+\pi^-$, K^+K^-: A touchstone of the perturbative QCD approach, *Phys. Rev. D* 99(1), 016019 (2019)
70. M. Beneke, V. M. Braun, Y. Ji, and Y. B. Wei, Radiative leptonic decay $B \to \gamma\ell\nu\ell$ with subleading power corrections, *J. High Energy Phys.* 2018(7), 154 (2018)
71. Y. M. Wang and Y. L. Shen, Subleading power corrections to the pion–photon transition form factor in QCD, *J. High Energy Phys.* 2017, 37 (2017), arXiv: 1706.05680 [hep-ph]
72. Y. M. Wang and Y. L. Shen, Subleading-power corrections to the radiative leptonic $B \to \gamma\ell\nu$ decay in QCD, *J. High Energy Phys.* 2018(5), 184 (2018)
73. C. D. Lü, Y. L. Shen, Y. M. Wang, and Y. B. Wei, QCD calculations of $B \to \pi$, K form factors with higher-twist corrections, *J. High Energy Phys.* 2019, 24 (2019), arXiv: 1810.00819 [hep-ph]
74. J. Gao, C. D. Lü, Y. L. Shen, Y. M. Wang, and Y. B. Wei, Precision calculations of $B \to V$ form factors from soft-collinear effective theory sum rules on the light-cone, *Phys. Rev. D* 101(7), 074035 (2020)
75. H. D. Li, C. D. Lü, C. Wang, Y. M. Wang, and Y. B. Wei, QCD calculations of radiative heavy meson decays with subleading power corrections, *J. High Energy Phys.* 2020, 23 (2020), arXiv: 2002.03825 [hep-ph]
76. Y. L. Shen, Z. T. Zou, and Y. B. Wei, Subleading power corrections to the $B \to \gamma\ell\nu$ decay in the perturbative

QCD approach, *Phys. Rev. D* 99(1), 016004 (2019)
77. Y. L. Shen, Z. T. Zou, and Y. Li, Power corrections to pion transition form factor in perturbative QCD approach, *Phys. Rev. D* 100(1), 016022 (2019)
78. Y. L. Shen, J. Gao, C. D. Lü, and Y. Miao, Power corrections to the pion transition form factor from higher-twist distribution amplitudes of a photon, *Phys. Rev. D* 99(9), 096013 (2019)
79. M. Beneke, P. Böer, J. N. Toelstede, and K. K. Vos, QED factorization of non-leptonic B decays, *J. High Energy Phys.* 2020, 81 (2020), arXiv: 2008.10615 [hep-ph]
80. M. Beneke, P. Böer, G. Finauri, and K. K. Vos, QED factorization of two-body non-leptonic and semi-leptonic B to charm decays, *J. High Energy Phys.* 2021(10), 223 (2021)
81. H. Y. Cheng and C. K. Chua, Revisiting charmless hadronic $B_{u,d}$ decays in QCD factorization, *Phys. Rev. D* 80(11), 114008 (2009)
82. M. Beneke, J. Rohrer, and D. Yang, Branching fractions, polarisation and asymmetries of $B \to VV$ decays, *Nucl. Phys. B* 774, 64 (2007), arXiv: hep-ph/0612290
83. C. Wang, Q. A. Zhang, Y. Li, and C. D. Lu, Charmless $B_s \to VV$ decays in factorization-assisted topological-amplitude approach, *Eur. Phys. J. C* 77(5), 333 (2017)
84. J. G. Körner and G. R. Goldstein, Quark and particle helicities in hadronic charmed particle decays, *Phys. Lett. B* 89(1), 105 (1979)
85. B. Aubert, et al. [BaBar], Rates, polarizations, and asymmetries in charmless vector–vector B decays, arXiv: hep-ex/0303020 (2003)
86. K. F. Chen, et al. [Belle], Measurement of branching fractions and polarization in $B \to \varphi K^*$ decays, *Phys. Rev. Lett.* 91(20), 201801 (2003), arXiv: hep-ex/0307014
87. Q. Qin, C. Wang, D. Wang, and S. H. Zhou, The factorization-assisted topological-amplitude approach and its applications, arXiv: 2111.14472 [hep-ph] (2021)